




Formation of $\text{Cd}_x\text{Pb}_{1-x}\text{S}/\text{Cd}_{1-\delta}\text{S}$ thin-film two-phase compositions by chemical bath deposition: composition, structure, and optical properties

L. N. Maskaeva^{1,2}, I. V. Vaganova^{1,2}, V. F. Markov^{1,2}, V. I. Voronin³, O. A. Lipina⁴, E. V. Mostovshchikova^{3,*} , V. S. Belov^{5,6}, and I. N. Miroshnikova^{5,7}

¹Ural Federal University, 19 Mira Str., 620002 Yekaterinburg, Russia

²Ural Institute of State Fire Service of EMERCOM of Russia, 22 Mira Str., 620062 Yekaterinburg, Russia

³M.N. Miheev Institute of Metal Physics of Ural Branch of Russian Academy of Sciences, 18 S. Kovalevskaya Str., 620108 Yekaterinburg, Russia

⁴Institute of Solid State Chemistry of the Ural Branch of the Russian Academy of Sciences, 91 Pervomaiskaya Str., 620990 Yekaterinburg, Russia

⁵Institute of Nanotechnology of Microelectronics of the Russian Academy of Sciences (IMNE RAS), 32A St. Leninsky Prospect, 119991 Moscow, Russia

⁶National Research University of Electronic Technology, 124498, Id. 1 Shokin Square, Zelenograd, Moscow, Russia

⁷National Research University "Moscow Power Engineering Institute", 14 Krasnokazarmennaya Str., 111250 Moscow, Russia

Received: 15 March 2021

Accepted: 18 June 2021

Published online:
30 June 2021

© The Author(s), under exclusive licence to Springer Science+Business Media, LLC, part of Springer Nature 2021

ABSTRACT

The possibility of forming thin-film two-phase compositions $\text{Cd}_x\text{Pb}_{1-x}\text{S}/\text{Cd}_{1-\delta}\text{S}$ using chemical bath deposition from aqueous media with adding various cadmium salts has been demonstrated. The crystal structure, chemical composition, morphology, and the band gap were studied by the X-ray diffraction, scanning electron microscopy, elemental analysis, Auger and Raman spectroscopy, and diffuse reflectance measurements. The formation of a $\text{Cd}_x\text{Pb}_{1-x}\text{S}/\text{Cd}_{1-\delta}\text{S}$ substitutional solid solution phase in well-faceted crystallites on the substrate of an X-ray amorphous CdS phase was experimentally shown. The observed difference in the composition of the films deposited with adding different cadmium salts is the result of the effect of the nucleophilicity of the anionic component of these salts on the kinetics of thiourea decomposition. The results demonstrate the possibility of forming thin-film two-phase compositions or heterostructures on the base of cadmium and lead sulfides in one technological stage using chemical bath deposition, which can be important for the creation of solar cells.

Address correspondence to E-mail: mostovsikova@imp.uran.ru

1 Introduction

For modern solar energy, the most interesting objects are thin-film solar cells in which absorbing layers are based on substitutional $\text{Cd}_x\text{Pb}_{1-x}\text{S}$ solid solutions. This is caused by the semiconducting properties of these compositions. Significant difference in the band gap value for the end members of the solid solution ($E_g = 0.41$ eV for PbS and $E_g = 2.4$ eV for CdS) provides wide range of spectral sensitivity variation [1–3]. For example, a model of the multiple band gap solar cells was proposed in [4], which were based on $\text{Cd}_x\text{Pb}_{1-x}\text{S}$ alloy nanowires of varying composition and delivered the efficiency higher than 40%. In recent papers [5–7] the possibility of the creation of the photovoltaic devices for solar cells on the base of heterojunction CdS/PbS with high performance was shown. Therefore, starting since 1970s the issue of the creation of devices for photovoltaic applications from PbS–CdS system is still topical. It should be mentioned, that one of the aims is a simplification of the process of formation of the working elements in such devices which can be achieved by the co-deposition of PbS and CdS in one process.

As it is shown in literature, there are different methods for producing $\text{Cd}_x\text{Pb}_{1-x}\text{S}$ films such as vacuum evaporation technique [8] and spray pyrolysis [9], method of ion-exchange substitution [10], sol–gel technology [11] or chemical bath deposition (CBD) from aqueous solutions [12–19]. The CBD method is of particular interest, because it is distinguished by instrumental simplicity and low-temperature conditions of the deposition process. The co-deposition of CdS and PbS makes it possible to obtain films of $\text{Cd}_x\text{Pb}_{1-x}\text{S}$ solid solutions with wide range of compositions having variable photoelectric characteristics. The composition of the films synthesized by the co-deposition of CdS and PbS is strongly determined by the specified conditions of the CBD process. For example, single-phase supersaturated substitutional $\text{Cd}_x\text{Pb}_{1-x}\text{S}$ solid solutions with different composition were obtained in [12–15]. In the same time, there are the papers, where two-phase films on the base of PbS and CdS were obtained. For example, E. Pentia et al. [16] revealed the presence in the deposited films two independent phases of PbS and CdS in addition to $\text{Cd}_x\text{Pb}_{1-x}\text{S}$ and noted that the experimental data obtained did not allow to conclude unambiguously that the deposited layers were only solid solutions of $\text{Cd}_x\text{Pb}_{1-x}\text{S}$ for the entire range of

x from 0 to 1. In [16], forming the solid solutions occurs only when the synthesis conditions are close to the deposition of phases of individual lead and cadmium sulfides; in other cases, a mechanical mixture $(\text{CdS})_x(\text{PbS})_{1-x}$ is deposited with different composition depending on the synthesis conditions. The close situation was observed in [20]: deposited films contained a virtually two-phase composition of individual sulfides $(\text{PbS})_{1-x}(\text{CdS})_x$, because there was not found continuous change in the lattice parameter and fundamental optical gap. Deo et al. [21] declared about the preparation of $\text{Cd}_{0.5}\text{Pb}_{0.5}\text{S}$ film, but there is a discrepancy between the reported composition of the solid solutions and the value of the band gap. Barote et al. [22] reported data on $\text{Cd}_{0.825}\text{Pb}_{0.175}\text{S}$ film, however only the peaks corresponding to CdS and PbS were shown in the X-ray diffraction patterns, therefore there was no experimental evidence of the formation of solid solutions. Paper of K.E. Suryavanshi et al. [19] also should be mentioned as paper in which formation of $\text{Pb}_x\text{Cd}_{1-x}\text{S}$ films with $0 \leq x \leq 1$ was reported. We would like to note that in our opinion the concentrations of the reagents taken by the authors are too high to prepare such reaction mixture for deposition of the single-phase film. Moreover, we do not see any evidence for formation of the substitutional solid solution like a shift of the X-ray diffraction peaks.

The results reported in [17, 18] attract the particular attention. In [17], it was found that single-phase state in the CBD films of $\text{Pb}_{1-x}\text{Cd}_x\text{S}$ with $x \leq 0.15$ (sometimes 0.18) is formed only at relatively low concentration of cadmium salt in the reaction bath. The increase in the cadmium salt concentration results in the deposition of X-ray amorphous CdS along with the solid solution. Thus, a two-phase system like $\text{Pb}_{1-x}\text{Cd}_x\text{S} + \text{CdS}$ is formed on the substrate. A similar result was obtained in [18], where two-phase layers containing 2–8 mol% of amorphous CdS phase in addition to $\text{Cd}_x\text{Pb}_{1-x}\text{S}$ solid solution were deposited on various substrates (silicon, siall, ITO coating, glass). Note that the phase segregation with the formation of two-phase films containing $\text{Cd}_x\text{Pb}_{1-x}\text{S}$ solid solution and X-ray amorphous CdS was established earlier upon isothermal annealing of supersaturated $\text{Cd}_x\text{Pb}_{1-x}\text{S}$ solid solutions when they were heated above 405–410 K [23]. The presented data indicate that upon the co-deposition of lead and cadmium sulfides during the CBD synthesis of Pb–Cd–S films, it is possible to form thin-film

compositions or heterostructures in one technological stage. The difference in the type of conductivity and photovoltaic properties of the phases formed in this case indicates the prospects for the creation of solar cells on their basis.

Let us also add that the analysis of works on the co-deposition of PbS and CdS and the phase composition of the obtained films shows that to ensure targeted synthesis it is important to take into account not only the complexing agents used in the system, but also the type of the anionic component of the cadmium salt [14]. Therefore, the aim of the present work was to carry out chemical bath deposition of three-phase films of the CdS–PbS system by using different cadmium salt and to study the composition, structure and optical properties to show the possibility of one-stage forming the compositions promising for using in solar radiation converters.

2 Experiment

Thin films on the base of lead and cadmium sulfides were synthesized by the chemical bath deposition from aqueous solutions containing 0.04 M of lead acetate $\text{Pb}(\text{CH}_3\text{COO})_2$, 0.3 M of sodium citrate $\text{Na}_3\text{C}_6\text{H}_5\text{O}_7$, 4.5 M of ammonium hydroxide NH_4OH , 0.58 M of thiourea $(\text{NH}_2)_2\text{CS}$, and 0.1 M of cadmium salt. To establish the effect of the anionic component of the cadmium salt, we used acetate $\text{Cd}(\text{CH}_3\text{COO})_2$, nitrate $\text{Cd}(\text{NO}_3)_2$, and sulfate CdSO_4 . At that, the main complexing agents for the metals regulating the rate of their precipitation were citrate ions for lead and ammonia for cadmium. The formulation used in the conditions of a competing process of formation of lead sulfide phase and cadmium sulfide one creates possibility for the deposition of the films inhomogeneous in composition, consisting of two or more phases. Binary sulfides PbS and CdS were obtained by excluding cadmium or lead salts from the reaction bath.

The deposition of the films was carried out at 353 K for 120 min in sealed reactors made from molybdenum glass, in which pre-degreased quartz substrates were fixed in fluoroplastic holders. The reactors were placed in a TC-TB-10 thermostat, which maintained the temperature of the reaction with the accuracy of $\pm 0.1^\circ$.

The thickness of the films was determined using an MII-4 M interference microscope (Linnik

Microinterferometer) with a measurement error of 20%. The thickness of the PbS film was about 600 nm; the thickness of the films deposited from the baths with adding cadmium salt was about 650–700 nm.

The crystal structure of the films was studied by X-ray diffraction (XRD) in the range of angles from 20 to 100 degrees, a step was $\Delta(2\theta) = 0.02$ degrees, a scan time was 10 s at a point. A PANalytical Empyrean Series 2 laboratory diffractometer with $\text{CuK}\alpha$ radiation was used. A position-sensitive PIXel3D detector in the parallel beam geometry provided the resolution on 2θ scale of at least 0.0016° . The structural parameters of the studied $\text{Cd}_x\text{Pb}_{1-x}\text{S}$ films were improved from experimental XRD patterns by the full-profile Rietveld analysis [24, 25] using the Fullprof program [26]. To separate the contributions of grain size and deformations in the studied films into the width of the diffraction peaks, the *conventional* Williamson–Hall plot equation was used [27]:

$$\beta \times \cos \Theta = 0.9\lambda/D + 4\varepsilon \times \sin \Theta, \quad (1)$$

where D is the average size of the coherent scattering regions (CSR), taken as the average particle size, β is the half-width of the peak in radians, λ is the wavelength of the X-ray radiation used, $\varepsilon = \Delta d/d$ is the deformation, d is the interplanar distance in Debye's formula $2d\sin\Theta = \lambda\sqrt{(h^2 + k^2 + l^2)}$.

The microstructure of the deposited films was studied by using a AMP-9510F Field Emission Auger Microprobe (JEOL). For SEM images, tilt angle of the sample relative to the electron beam was 0 degrees; the accelerating voltages of electrons were 10 and 30 keV, the beam current was 0.2 nA, and the electron beam diameter was less than 10 nm. Elemental composition of the films was determined by a JEOL JSM-5900 LV scanning electron microscope with an energy-dispersive X-ray (EDX) analyzer EDS Inca Energy 250.

The Auger spectra of the studied films before and after etching were obtained by using a JEOL Jamp-9510F Auger-electron spectrometer. The energy of the primary electron beam was 10 keV. The angle of inclination of the sample relative to the normal to the primary electron beam was 30 degrees. The diameter of the electron beam during profiling was more than 100 μm and less than 10 nm when analyzed from a point. An argon ion gun with the energy 2000 eV was used to obtain a depth profile. The etching rate was in the range of 3–12 nm/min.

The Raman spectra were recorded on a RENISHAW-1000 spectrometer (Renishaw plc., UK) equipped with a Leica DML confocal microscope, a notch filter, a CCD camera, and a LCM-S-111 solid-state laser with the radiation wavelength of 532 nm. The spectral resolution was $1\text{--}2\text{ cm}^{-1}$, the laser beam size was $1\text{ }\mu\text{m}$, the exposure time of one spectrum varied from 20 to 30 s, the number of scans (the number of signal accumulation cycles) was two.

The diffuse reflectance study of the films was carried out on a UV-3600 spectrometer (Shimadzu, Japanese) equipped with an ISR-3100 integration sphere. The reflectance spectra $R(\lambda)$ were recorded in the range of 220–2000 nm with the scanning step of $\Delta\lambda = 1\text{ nm}$. BaSO_4 was used as a reflectance standard. The optical band gap energy (E_g) of the phases forming the studied $\text{Cd}_x\text{Pb}_{1-x}\text{S}$ film was evaluated by the method proposed by Kubelka and Munk–Aussig [28]. The Kubelka–Munk function was calculated by the equation:

$$F(R_\infty) = \frac{(1 - R_\infty)^2}{2R_\infty} = \frac{k}{s}, \quad (2)$$

where R_∞ was the diffuse reflectance of an infinitely thick sample relative to the reference, k was the molar absorption coefficient, and s was the scattering coefficient.

3 Results and discussion

3.1 Structure

Figure 1 shows the experimental and calculated XRD patterns for the synthesized PbS film and the compositions on the base of PbS and CdS. The experimental profile of the XRD patterns was described using a crystal lattice model of the rock salt NaCl type B1 ($Fm\bar{3}m$ space group) by varying the lattice parameter, atomic coordinates, filling positions, as well as background, shape, and width of the reflexes. Corrections for the preferred orientation of grains and anisotropy were introduced, if necessary. Internal microstrains and size of CSR in isotropic and anisotropic versions were calculated on the basis of the Williamson–Hall extrapolation equation (1).

The XRD pattern of the individual PbS film contains only peaks of a cubic face-centered lattice of the NaCl type (B1). The diffraction patterns of the films deposited from the baths containing cadmium salt

also show the main diffraction reflections of the B1 cubic phase. The angular positions of the reflections of the B1 phase are shown in Fig. 1 by dashes. It should be noted that the diffraction patterns of the films obtained from the baths with adding cadmium salt are more complex than that of the individual PbS film (Fig. 1b–d). It is clearly seen that, instead of the isotropic background (Fig. 1a), the XRD patterns of the films with cadmium have a strong diffuse halo from the amorphous material, as well as sets of peaks from the additional crystalline phase with hexagonal structure B4 ($P6_3mc$ space group) corresponding to cadmium sulfide.

Figure 2 shows the fragments of the XRD patterns near (111) peak of B1 phase for the films deposited from the mixtures containing $\text{Cd}(\text{CH}_3\text{COO})_2$, $\text{Cd}(\text{NO}_3)_2$, or CdSO_4 . The intensity of the additional reflections corresponding to the B4 phase in the films is almost the same, which indicates close portion of CdS phase. The experimental parameters of the unit cell of hexagonal cadmium sulfide ($a = 0.4048\text{--}0.4071\text{ nm}$, $c = 0.6480\text{--}0.6581\text{ nm}$) are somewhat lower than the values given in the literature [29] ($a = 0.4094\text{ nm}$, $c = 0.6709\text{ nm}$). This may be caused by a nonstoichiometry of $\text{Cd}_{1-\delta}\text{S}$ phase. Another reason for difference between the lattice parameters of cadmium sulfide determined in the present work and represented in the literature can be the fact that during the formation of this phase the compression of the thin-film layer occurs under the external pressure as a result of the difference between the volumes of the crystal lattices of the quartz substrate and the synthesized films. A similar effect of a decrease in the parameters and volume of the unit cell was found for a single crystal of hexagonal CdS [30].

The diffraction patterns show that the films under study are polycrystalline. To describe the XRD pattern of the pure PbS layer, a single-phase model was used; a broadening of reflexes was taken into account and a correction for texturing was introduced. The analysis of the diffraction patterns of the cadmium-contained films was carried out taking into account diffuse scattering from an amorphous material in a two-phase model. The regions of the X-ray patterns with instrumental peaks were excluded from consideration. In addition, a model with anisotropic broadening of reflections of the main B1 phase was used. The use of such models increases the accuracy in describing the profiles of the experimental XRD

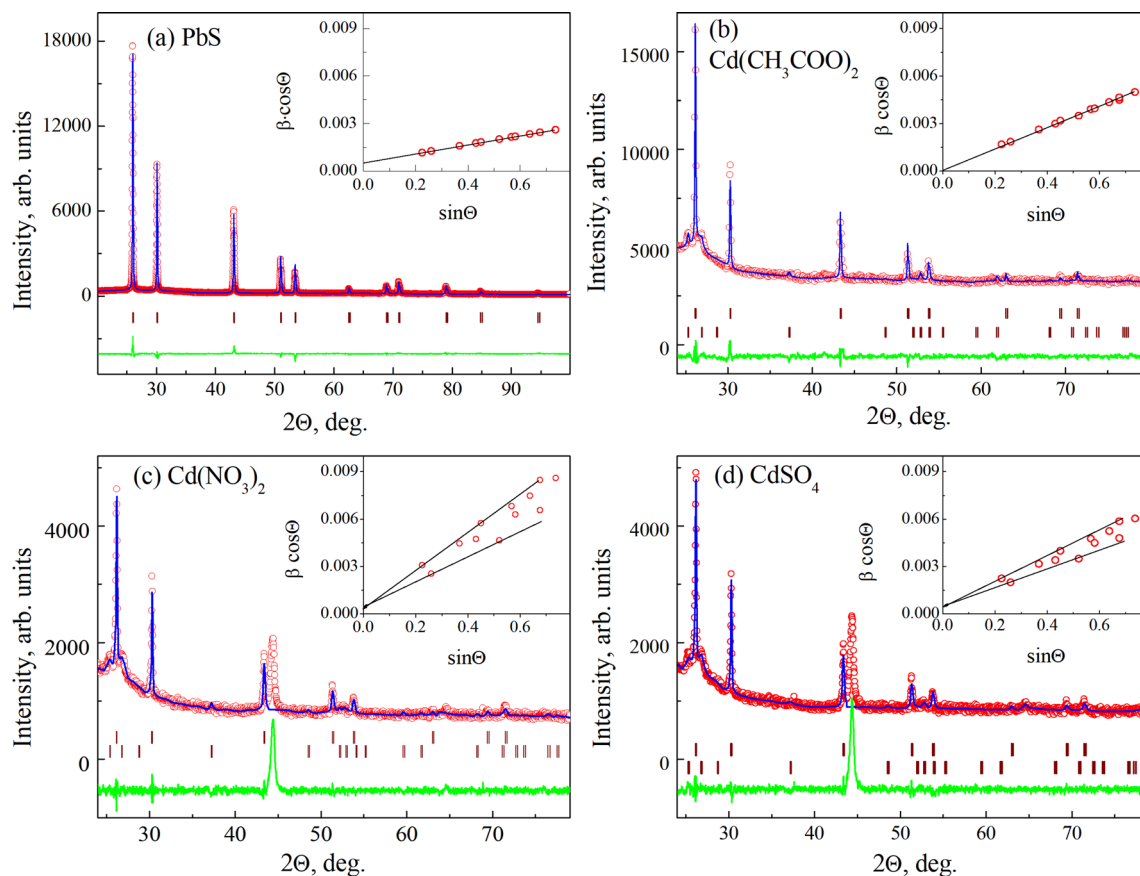


Fig. 1 Experimental (red circles) and calculated (blue envelope lines) XRD patterns of initial PbS films (a) and $\text{Cd}_x\text{Pb}_{1-x}\text{S}$ films deposited from the reaction bath containing $\text{Cd}(\text{CH}_3\text{COO})_2$ (b), $\text{Cd}(\text{NO}_3)_2$ (c), and CdSO_4 (d). The bottom line (green) is the difference between calculation and experiment. Dashes show the

angular positions of the reflections of the B1 phase (upper on b, c, d) and the hexagonal B4 phase (lower on b, c, d). Insets show $\beta(2\theta) \cos \theta$ versus $\sin \theta$ dependences on the same scale for easy comparison (Color figure online)

patterns and, accordingly, the structural parameters of the films of $\text{Cd}_x\text{Pb}_{1-x}\text{S}$ solid solutions. The difference between the experimental and calculated X-ray patterns for the films in Fig. 1 confirms the high accuracy of the full-profile analysis performed.

Comparison of the XRD patterns of the studied cadmium-containing films and the PbS one shows that adding cadmium results in a shift of all peaks to the region of larger angles 2θ . This shift is accompanied by a slight decrease in the period a_{B1} of the PbS cubic lattice upon replacement of lead with cadmium from $a_{B1} = 0.59348$ nm to 0.59028 ($\text{Cd}(\text{CH}_3\text{COO})_2$), 0.59012 ($\text{Cd}(\text{NO}_3)_2$), and 0.58986 nm (CdSO_4) (Table 1). A quantitative analysis of the diffraction patterns performed using the FullProf software package makes it possible to interpret the

observed decrease in the a_{B1} period of the cubic lattice as the formation of a $\text{Cd}_x\text{Pb}_{1-x}\text{S}$ solid solution with replacing Pb^{2+} ions with a radius $r_{\text{Pb}^{2+}} = 0.119$ nm by smaller Cd^{2+} ions with $r_{\text{Cd}^{2+}} = 0.097$ nm [31]. It should be noted that, due to the small thickness of the films and the presence of the texture, the cadmium concentration cannot be determined from the calculation of the experimental intensities of the XRD peaks. Therefore, the compositions of the solid solutions were estimated from the change in the lattice parameter using Vegard's rule [32], according to which the molar fraction of cadmium is determined as

$$x = (a_{\text{PbS}} - a_{\text{SS}}) / (a_{\text{PbS}} - a_{\text{CdS}}). \quad (3)$$

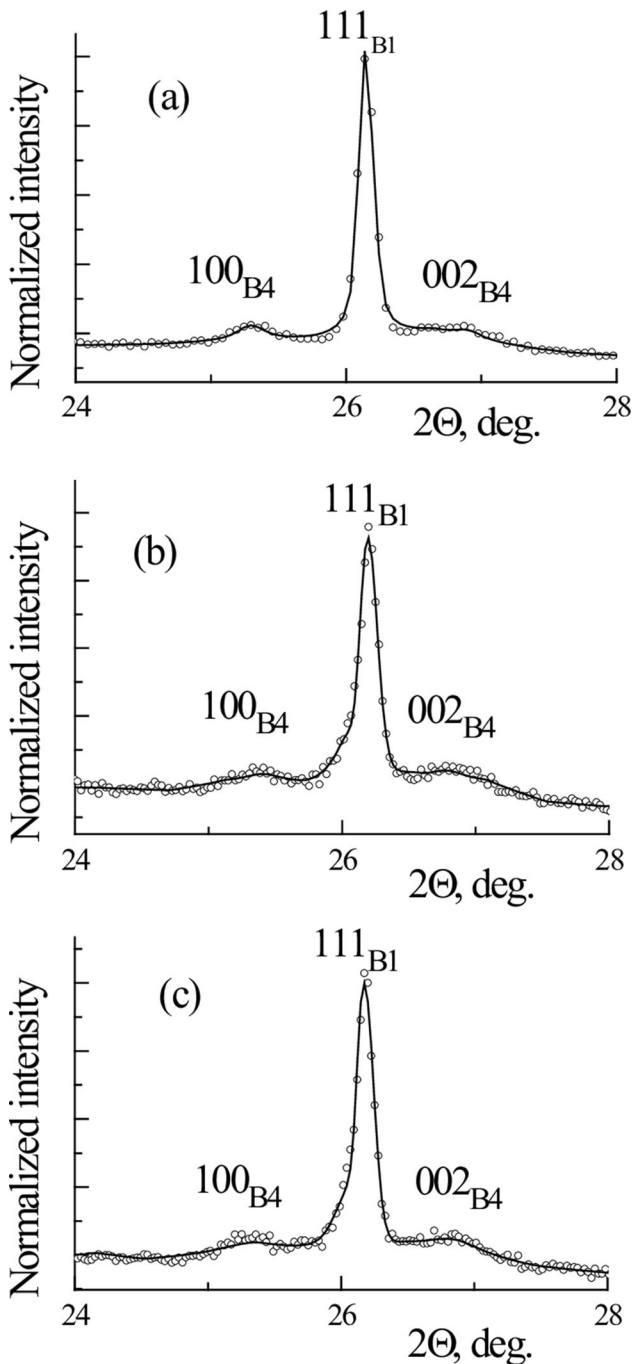


Fig. 2 Fragments of XRD patterns of the films synthesized from the reaction mixtures containing $\text{Cd}(\text{CH}_3\text{COO})_2$ (a), $\text{Cd}(\text{NO}_3)_2$ (b), and CdSO_4 (c). The intensities of the XRD peaks are normalized

Here, a_{PbS} , a_{CdS} , a_{SS} are the parameters of the crystal lattices of lead sulfide, cadmium sulfide, and substitutional $\text{Cd}_x\text{Pb}_{1-x}\text{S}$ solid solution. This rule is valid for isostructural compounds. Under normal

conditions, the crystal lattice of CdS is of the type of sphalerite (B3) or wurtzite (B4). Although sphalerite has a cubic lattice, cadmium cations are in the tetrahedral environment (the coordination number is 4). At the same time, in the PbS lattice, the environment of lead cations, and, consequently, of the cadmium cations replacing them, is octahedral (the coordination number is 6), which excludes the use of the sphalerite lattice parameter for determining the concentration x of Cd atoms in the $\text{Cd}_x\text{Pb}_{1-x}\text{S}$ solid solution. According to [33–36], the unit cell period of synthesized CdS with a NaCl crystal structure is 0.546 nm; we have used this value to calculate the cadmium content in the $\text{Cd}_x\text{Pb}_{1-x}\text{S}$ solid solutions. Using estimates made by minimizing XRD patterns, on the one hand, and changes in the lattice period, on the other hand, we have determined following compositions of the synthesized solid solutions: $\text{Cd}_{0.067}\text{Pb}_{0.933}\text{S}$ (cadmium acetate), $\text{Cd}_{0.071}\text{Pb}_{0.929}\text{S}$ (cadmium nitrate), $\text{Cd}_{0.076}\text{Pb}_{0.924}\text{S}$ (cadmium sulfate).

It can be seen that according to the degree of enrichment of the solid solution with cadmium, the salts used in the reaction mixture can be arranged in the following order: $\text{CdSO}_4 \rightarrow \text{Cd}(\text{NO}_3)_2 \rightarrow \text{Cd}(\text{CH}_3\text{COO})_2$. The given sequence of salts accords with the degree of their nucleophilicity manifesting the surface charge density and corresponds to the general lyotropic series of anions in their composition [37]. In [37], the concept was proposed about the activation of thiourea due to the nucleophilic addition of anions to the carbon atom in its composition with the formation of an intermediate reaction complex “thiourea $(\text{NH}_2)_2\text{CS}$ —metal ion (Cd^{2+}) —nucleophile $(\text{SO}_4^{2-}, \text{NO}_3^-, \text{CH}_3\text{COO}^-)$ ”. An increase in the reactivity of thiourea in this case will more affect the rate of formation of cadmium sulfide due to the more significant polarization of the carbon–sulfur bond in its complex with cadmium. This will affect the redistribution of the rates of formation of individual sulfide phases in favor of the cadmium sulfide, increasing the proportion of CdS in the composition of the solid solution in the established above sequence.

As we have mentioned, studied PbS and $\text{Cd}_x\text{Pb}_{1-x}\text{S}$ films are polycrystalline. The analysis of the intensities of diffraction peaks of the PbS film shows that the intensities of experimental reflections from planes of (hhh) type are higher than calculated ones for powder sample with the same composition. This indicates the presence of a preferred orientation of

Table 1 Crystal lattice parameter (a), cadmium concentration (x) in $\text{Cd}_x\text{Pb}_{1-x}\text{S}$, percentage of crystallites with a preferred orientation (111) parallel to the substrate plane ($T_{(111)}$), microstrains along differentcrystallographic directions ($\Delta d/d$) and average values of microstrains over the sample volume ($\langle \Delta d/d \rangle$), the size of the coherent scattering regions (D)

Film	PbS	$\text{Cd}(\text{CH}_3\text{COO})_2$		$\text{Cd}(\text{NO}_3)_2$		CdSO_4	
		B1	B4	B1	B4	B1	B4
a (nm) \pm 0.00001	0.59348	0.59028	$a = 0.4071$ $c = 0.6480$	0.59012	$a = 0.4049$ $c = 0.6578$	0.58986	$a = 0.4048$ $c = 0.6581$
x , in $\text{Cd}_x\text{Pb}_{1-x}\text{S}$	0	0.067	–	0.071	–	0.076	–
$T_{(111)}$, %	36.2	37.5	–	34.6	–	36.6	–
$\Delta d/d$, $\times 10^{-4}$							
(111)	10.3	16.4		31.5		28.2	
(200)	10.3	15.6		23.8		20.0	
(220)	10.3	16.2		29.7		26.4	
(311)	10.3	16.0		27.7		24.2	
(331)	10.3	16.2		30.3		26.9	
(422)	10.3	16.2		29.7		26.4	
$\langle \Delta d/d \rangle$, $\times 10^{-4}$	10.3	16.1	–	28.5	–	27.8	–
D , nm	254	~ 1000	33	330	17	312	7.5

grains in the plane of the film. By introducing a texture correction $T_{(111)}$ into the calculation, it was found that the grains are partially ($\sim 36\%$) ordered by (111) crystallographic plane along the substrate plane. The preferred orientation of the grains in the two-phase films also is of (111) type; the portion of the oriented grains is about 34.6–37.5%, which is close to the PbS film.

The broadening of all diffraction reflections is observed in the XRD patterns of the two-phase $\text{Cd}_x\text{Pb}_{1-x}\text{S}$ films. As an example, Fig. 3 shows the experimental and reference form of the reflection (311) of the layers under discussion. When analyzing the X-ray diffraction patterns of the synthesized films, two reasons for the broadening of diffraction reflections were considered: the small size of the coherent scattering regions D and internal microstrains $\Delta d/d$. Plotting the dependence $\beta(2\Theta) \times \cos\Theta = f(\sin\Theta)$ according to the Williamson–Hall equation [23] lets to make a conclusion about the reason for the XRD peaks broadening. Insets in Fig. 1 show these dependences in the same scale. It is seen that the experimental points of $\beta(2\Theta) \times \cos\Theta$ versus $\sin\Theta$ for the PbS film fit in a straight line with small angle of inclination indicating the existence of the microstrains in the film; the line intersects the ordinate axis above zero point, which points at a small size of CSR. The fact that all experimental points fit one line in $\beta(2\Theta) \times \cos\Theta$ versus $\sin\Theta$ coordinates evidences

isotropic character of the microstrains and CSR. For the film deposited from the reaction mixture containing cadmium acetate the line with experimental points (corresponding the $\text{Cd}_x\text{Pb}_{1-x}\text{S}$ phase) on the same dependence has greater angle inclination and the segment cut off by the line decreases. This indicates an increase in the microstrains and CSR. For the films deposited from baths with cadmium nitrate or cadmium sulfate, the angle of inclination of the linear dependence $\beta(2\Theta) \times \cos\Theta = f(\sin\Theta)$ and the segments cut off on the ordinate axis changes and the experimental points deviate from the average linear dependence. The observed irregularity in the arrangement of the experimental points can be a consequence of the presence of the anisotropy of microstrains along different crystallographic directions. Indeed, connecting the points corresponding to the crystallographic directions $[hhh]$ and $[h00]$ by a straight line one can see the different angle, which evidences different magnitudes of microstrains along these directions (insets in Fig. 1c, d). Ungar et al. [38, 39] believe that the broadening of reflections associated with the deformation anisotropy in films can be caused by the presence of defects and dislocations. At the same time, the straight lines drawn converge at one point on the ordinate axis determining the CSR size and representing the isotropic (near spherical) shape of the grains, which form the film.

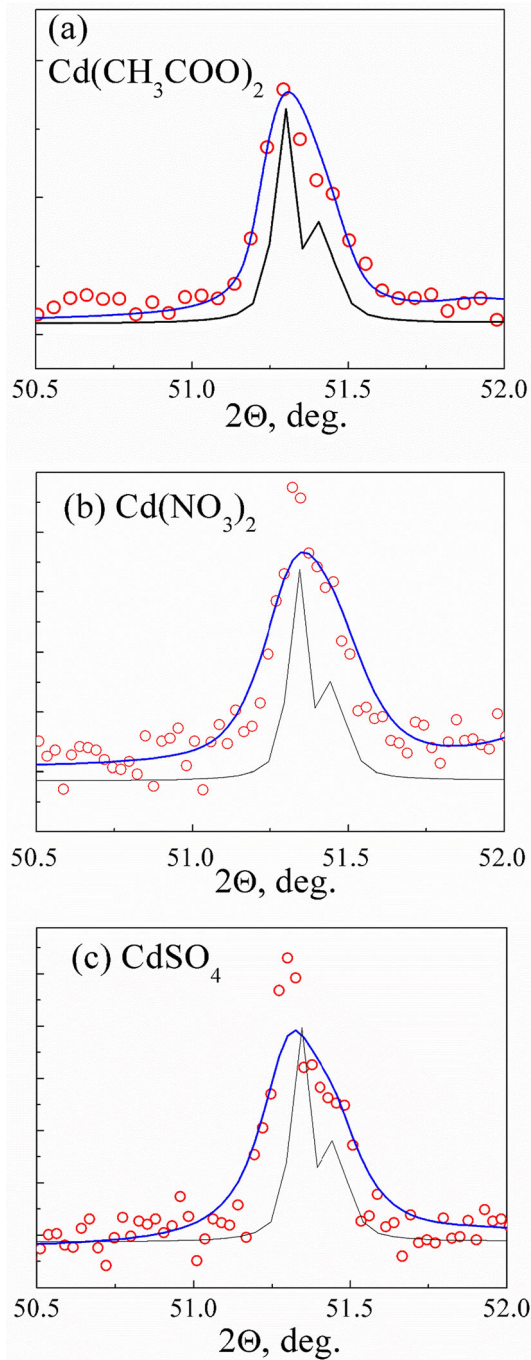


Fig. 3 Experimental (311) XRD peak of two-phase $\text{Cd}_x\text{Pb}_{1-x}\text{S}$ films (circles), deposited from the reaction baths with adding $\text{Cd}(\text{CH}_3\text{COO})_2$ (a), $\text{Cd}(\text{NO}_3)_2$ (b), CdSO_4 (c); the black line inside the peak corresponds to the reference sample reflection (Color figure online)

The sizes of CSR estimated from analysis of $\beta(2\Theta) \times \cos\Theta = f(\sin\Theta)$ dependences differ for the individual PbS film and for the two-phase films

containing $\text{Cd}_x\text{Pb}_{1-x}\text{S}$ solid solution. In the PbS film the value of D is the lowest. In the films with cadmium, CSR are largest in films deposited with $\text{Cd}(\text{CH}_3\text{COO})_2$ ($D \sim 1000$ nm) and smaller in the films with $\text{Cd}(\text{NO}_3)_2$ ($D = 320$ nm) or with CdSO_4 ($D = 312$ nm). Similar estimation of CSR was made for the $\text{Cd}_{1-\delta}\text{S}$ phase. It is found that the size of CSR of the $\text{Cd}_{1-\delta}\text{S}$ phase decreases from 33 nm for $\text{Cd}(\text{CH}_3\text{COO})_2$ to 17 nm for $\text{Cd}(\text{NO}_3)_2$ and 7.5 nm for CdSO_4 .

The microstrains are rather small and isotropic in the individual PbS film ($\Delta d/d = 10.3 \times 10^{-4}$). In the $\text{Cd}_x\text{Pb}_{1-x}\text{S}$ solid solution in film obtained from the bath containing cadmium acetate the microstrains increase insignificantly to $\Delta d/d = 16.1 \times 10^{-4}$ and anisotropy in the distribution of microstrains along crystallographic directions appears (Table 1). Using $\text{Cd}(\text{NO}_3)_2$ or CdSO_4 salts in the synthesis of the films results in an increase in $\Delta d/d$ value (to 28.5×10^{-4} and 27.8×10^{-4} , respectively); the anisotropy of microstrains becomes more pronounced (Table 1). This is also clearly seen in insets in Fig. 1.

As it was reported above, the observed peculiarities of the crystal structure of the films under study are a consequence of different degrees of activation of thiourea as a result of nucleophilic addition of anions and different stability of the intermediate reaction complexes formed in the system “ $\text{Me}^{2+}-(\text{NH}_2)_2\text{CS}-\text{An}^{n-}$ (SO_4^{2-} , NO_3^- , CH_3COO^-)” under the conditions of the competitive nature of the interaction of cadmium and lead with thiourea.

3.2 Morphology

Figure 4 shows the scanning electron microscope (SEM) images of the individual PbS film, the films of the two-phase compositions $\text{Cd}_x\text{Pb}_{1-x}\text{S}/\text{Cd}_{1-\delta}\text{S}$ obtained from the reaction mixtures with various cadmium salts, and the CdS film. It is seen, that there is significant change in the film morphology when cadmium salt is added into the bath. The PbS film is formed from the regular cut and tightly packed crystallites with the size of about 200–600 nm (Fig. 4a). The thin film of CdS have loose structure (Fig. 4b) because this film is formed from nonuniform globules with the size of 250–300 nm, and these globules are formed from small (20–30 nm) near spherical particles. The two-phase $\text{Cd}_x\text{Pb}_{1-x}\text{S}/\text{Cd}_{1-\delta}\text{S}$ compositions consist of the polyhedral crystallites with size of 200–1000 nm, which unevenly

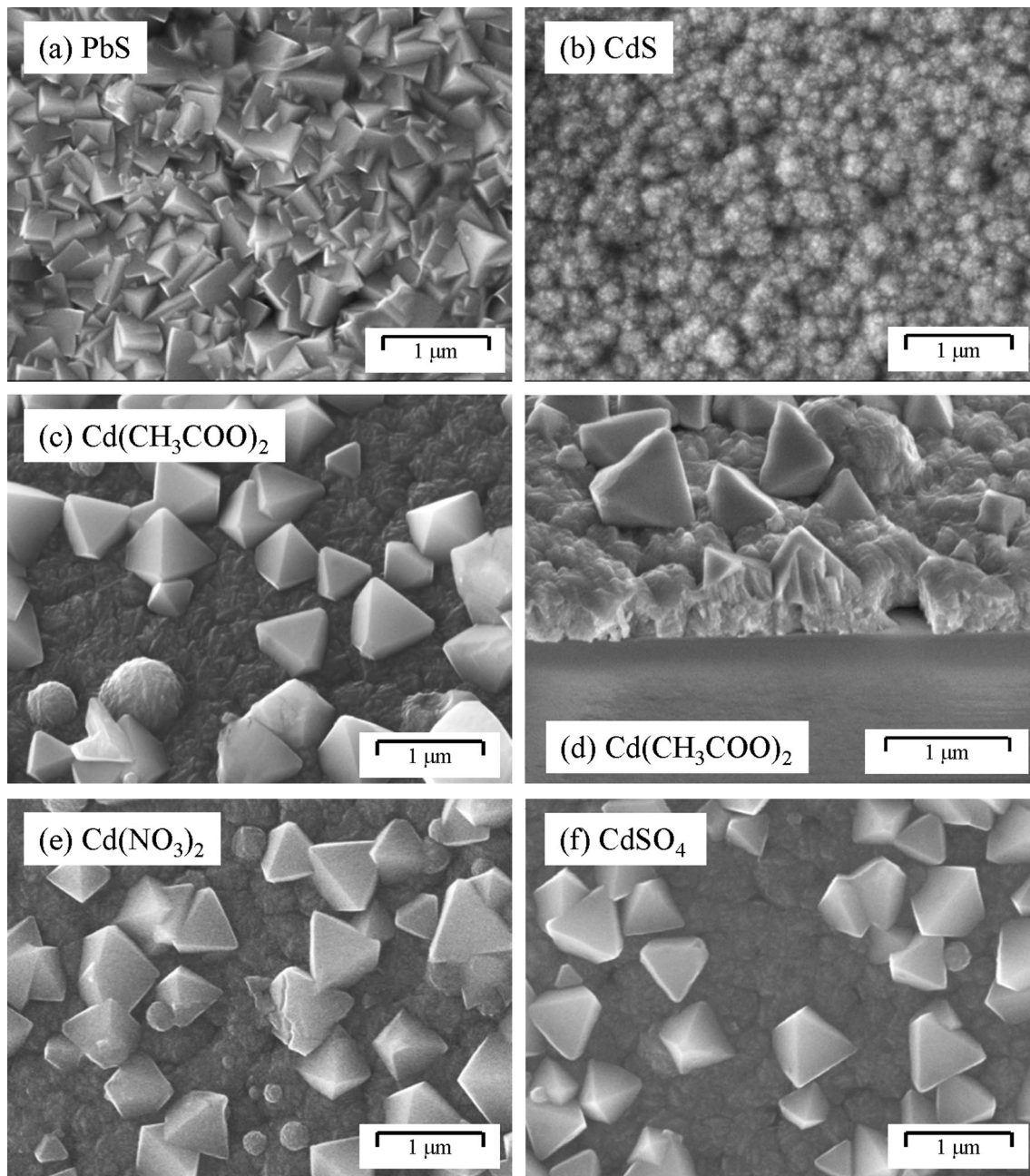


Fig. 4 Scanning electron microscope images of PbS (a), CdS (b), and two-phase $\text{Cd}_x\text{Pb}_{1-x}\text{S}/\text{Cd}_{1-\delta}\text{S}$ films deposited from the reaction baths containing $\text{Cd}(\text{CH}_3\text{COO})_2$ (c, d), $\text{Cd}(\text{NO}_3)_2$ (e),

CdSO_4 (f). Figure (d) shows the cross-section image for the film obtained using $\text{Cd}(\text{CH}_3\text{COO})_2$

distributed over the surface of the layer formed from globules. The size of the globules in sublayer is in the range of 300–700 nm for $\text{Cd}(\text{CH}_3\text{COO})_2$ (Fig. 4c, d) and 150–300 nm for $\text{Cd}(\text{NO}_3)_2$ (Fig. 4e). The sublayer in the two-phase film synthesized from the bath with CdSO_4 is an amorphous phase, which has the structure similar to the CdS film (compare Fig. 4b, f) and

does not contain globular formations. For a clearer understanding the microstructure of the two-phase compositions, Fig. 4d shows as an example the cross-section image for the $\text{Cd}_x\text{Pb}_{1-x}\text{S}/\text{Cd}_{1-\delta}\text{S}$ film obtained using $\text{Cd}(\text{CH}_3\text{COO})_2$. Let us to remind, that, as it follows from the analysis of the XRD data, the initial PbS film and the two-phase $\text{Cd}_x\text{Pb}_{1-x}\text{S}/\text{Cd}_{1-\delta}\text{S}$

compositions are characterized by a texture in which the crystallites are oriented by (111) plane along the substrate. Visually this manifests itself as crystallites directed by the cube apex perpendicular to the plane of the substrate.

According to the local elemental analysis data, the individual PbS film contains 49.7 ± 0.4 at.% of lead and 50.3 ± 0.4 at.% of sulfur, i.e., in terms of stoichiometry, there is a deficiency of metal. In turn, the CdS film contains some excess of metal: the film contains, on average, 51.6 ± 0.8 at.% of cadmium and 48.4 ± 0.8 at.% of sulfur. The elemental analysis of the two-phase $\text{Cd}_x\text{Pb}_{1-x}\text{S}/\text{Cd}_{1-\delta}\text{S}$ compositions was carried out for the crystallites, sublayer (intercrystalline space) and globular formations (for the film synthesized from the reaction bath containing $\text{Cd}(\text{CH}_3\text{COO})_2$); the results of the EDX analysis are represented in Table 2. The globular formations in the films deposited at presence of $\text{Cd}(\text{NO}_3)_2$ or CdSO_4 in the reaction bath were not analyzed because of their small size. The EDX data show that the content of the main elements (Cd, Pb, S) in the crystallites, globules and in the intervals between them differs significantly. At that in the crystallites in the two-phase compositions there is a certain excess in the anion content (50.1–50.7 at.%) in comparison with the sum of metals (Cd+Pb). Similar excess of sulfur was found for the intercrystalline space in the films synthesized using cadmium nitrate and sulfate; the sulfur content was 51.6 and 50.7 at.%, respectively. In contrast, in the film formed in the presence of cadmium acetate a deficiency of chalcogen (sulfur) was determined both in the intercrystalline space (48.9 at.%) and in globular formations (49.5 at.); in the intercrystalline space 1.6 at.% of lead was observed in addition to cadmium and sulfur.

Comparing results of the EDX analysis for the crystallites in the two-phase compositions (Table 2) and the chemical composition of the $\text{Cd}_x\text{Pb}_{1-x}\text{S}$ solid solutions of these films estimated from XRD data

(Table 1), the difference between the concentrations of cadmium is seen. There is a number of the reasons for observed difference. The first one is the fact, that the penetration depth of the electron beam in the EDX analysis is greater than the thickness of the films under study, i.e., an amorphous sublayer of cadmium sulfide is analyzed simultaneously with the crystallites. The second reason of the observed excess of the content of the substituting component can be associated with the presence of the CdS island formations on the faces of the crystallites as it was shown in [40]. As the last reason of the difference between cadmium content determined by EDX and XRD, we assume that part of cadmium ions occupies interstitial positions. If cadmium ions occupy intersects, the lattice parameter should be higher than the parameter in the case when all cadmium ions are in the lead positions, therefore the content of cadmium is underestimated. There are many examples of the appearance of the interstitial solutions when PbS is doped with elements with smaller size. For example, in work [41] it was shown that an increase or a decrease in the PbS lattice parameter upon doping with Hg was associated with a change in the distribution of mercury atoms in the lattice which was substitution or insertion, respectively.

3.3 Auger spectroscopy

For a more detailed study of the elemental composition of the films near the surface and at a certain depth, the Auger electron spectroscopy (AES) was used. The survey Auger spectra recorded from the surface of all the films under study show the presence of oxygen atoms associated with the surface oxidation and carbon atoms due to the natural surface contamination. To remove the carbon impurities and the oxidized layer, the films were etched for 1 min to a depth of 5 nm with argon ions. After ion etching, the survey Auger spectra shown in Fig. 5 indicate the

Table 2 Results of EDX analysis of two-phase $\text{Cd}_x\text{Pb}_{1-x}\text{S}/\text{Cd}_{1-\delta}\text{S}$ compositions

Analysis area	$\text{Cd}(\text{CH}_3\text{COO})_2$			$\text{Cd}(\text{NO}_3)_2$			CdSO_4		
	Elements, at.%								
	Pb	Cd	S	Pb	Cd	S	Pb	Cd	S
Crystallites	42.9	7.0	50.1	42.5	7.2	50.3	41.8	7.5	50.7
Globules	32.1	18.4	49.5	–	–	–	–	–	–
Intercrystalline space	1.6	49.5	48.9	–	48.4	51.6	–	49.3	50.7

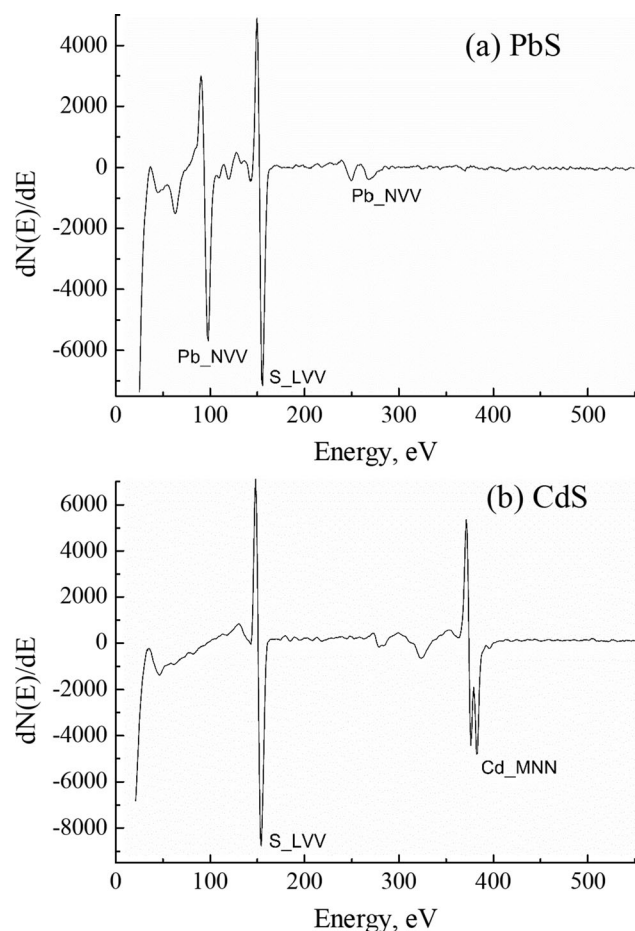


Fig. 5 Differential survey Auger spectra of the surface of PbS (a) and CdS (b) at a depth of 30 nm after ion etching

absence of carbon and oxygen atoms in the depth of the studied films (the detection limit of carbon and oxygen is about 1 at.%).

Figure 5a shows the Auger spectrum of the PbS film with a narrow peak in the low-energy range (90–94 eV) and a weak peak in the middle energy range (249–267 eV) associated with lead ions [42]. In the spectrum of CdS (Fig. 5b) there are peaks at 376 and 382 eV attributed to cadmium ions [42, 43]. Besides this, in the spectra the peak at 152 eV is seen, which is connected with sulfur ions. These spectra of the binary compounds were used for the interpretation of the atomic depth profile for the two-phase $\text{Cd}_x\text{Pb}_{1-x}\text{S}/\text{Cd}_{1-\delta}\text{S}$ compositions considered in the present work.

As seen from the SEM images (Fig. 4), the surfaces of the two-phase compositions have a complex structure with light crystallites lying on a dark

amorphous CdS sublayer. Therefore, these regions were analyzed by AES. Figure 6 shows the Auger spectra of the amorphous sublayer (intercrystalline space) (left panels) and crystallites (right panels) in the two-phase $\text{Cd}_x\text{Pb}_{1-x}\text{S}/\text{Cd}_{1-\delta}\text{S}$ compositions after the ion etching at a depth of 30 nm. To ensure precise recording of the AES curves of crystallites and sublayer of the films, the “Probe tracking” function was used, which corrected the position of the analysis point, the shift from which did not exceed 20 nm. As a result, the displacement of the electron beam from the large crystallite to the amorphous layer and vice versa was excluded. From the comparison of the Auger spectra of the two-phase $\text{Cd}_x\text{Pb}_{1-x}\text{S}/\text{Cd}_{1-\delta}\text{S}$ compositions (Fig. 6) and the binary compounds PbS and CdS (Fig. 5), the peaks corresponding to lead, cadmium, and sulfur are clearly identified. At that, the intensities of the Auger signals of cadmium and lead in the large crystallites and the amorphous layer differ at a similar intensity of the signal of sulfur. The ratios of the intensities of the peaks responsible for the presence of the discussed atoms depend on the cadmium salt used in the reaction bath. The determination of the elemental composition of the crystallites of the two-phase $\text{Cd}_x\text{Pb}_{1-x}\text{S}/\text{Cd}_{1-\delta}\text{S}$ compositions and the amorphous sublayer was carried out assuming a homogeneous distribution of elements in the analyzed parts of the films and using the intensities of the Auger peaks of the binary CdS and PbS films with an identical matrix and a known concentration of atoms of the studied elements. This made it possible to determine the difference between the films under study, taking into account possible analysis errors.

For the $\text{Cd}_x\text{Pb}_{1-x}\text{S}/\text{Cd}_{1-\delta}\text{S}$ film deposited from the reaction bath with adding $\text{Cd}(\text{CH}_3\text{COO})_2$, the concentration of lead in the crystallites is estimated as 39 ± 6 at.%, the content of cadmium is 10 ± 2 at.%, and the sulfur concentration is 51 ± 8 at.%. At the same time in the regions of the film between the crystallites the content of cadmium, lead and sulfur is determined as 46 ± 7 at.%, 7 ± 1 at.%, and 47 ± 7 at.%, respectively. For the films synthesized from the reaction mixture with $\text{Cd}(\text{NO}_3)_2$ or CdSO_4 the content of the elements in the crystallites and sublayer differs in comparison with the previously mentioned two-phase film (Table 3). The concentration of the cadmium increases in the crystallites and decreases in the sublayer (the places between the crystallites)

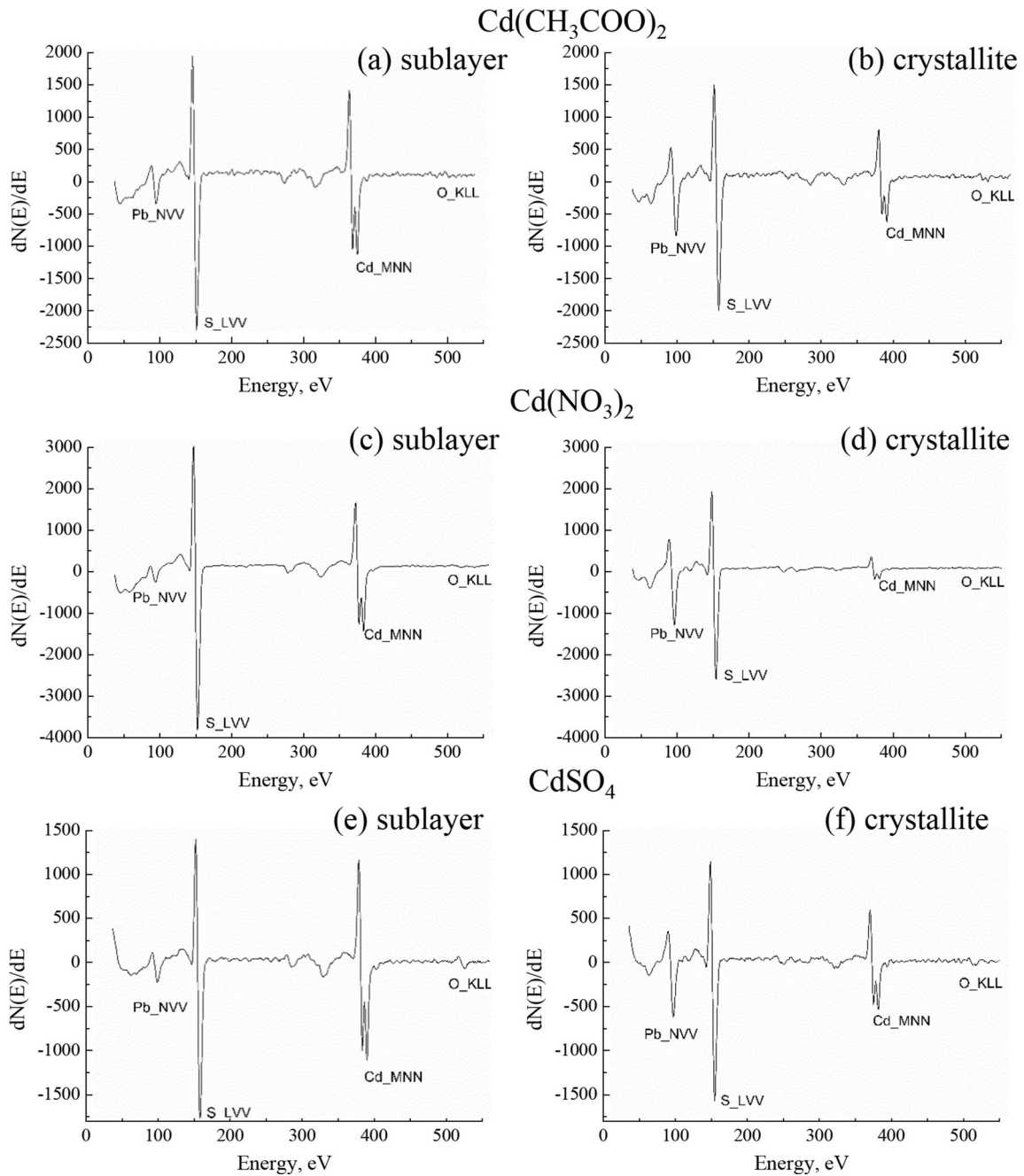


Fig. 6 Differential survey Auger spectra of the surface of intercrystalline space (sublayer) (a, c, e) and crystallites (b, d, f) of two-phase Cd_xPb_{1-x}S/Cd_{1-δ}S films, deposited from the

reaction bath with adding Cd(CH₃COO)₂ (a, b), Cd(NO₃)₂ (c, d), CdSO₄ (e, f) at a depth of 30 nm after ion etching

Table 3 Results of elemental analysis of two-phase Cd_xPb_{1-x}S/Cd_{1-δ}S compositions by Auger spectroscopy

Analysis area	Cd(CH ₃ COO) ₂			Cd(NO ₃) ₂			CdSO ₄		
	Elements, at. %								
	Pb	Cd	S	Pb	Cd	S	Pb	Cd	S
Crystallites	39 ± 6	10 ± 2	51 ± 8	35 ± 5	14 ± 2	51 ± 8	32 ± 4	16 ± 2	52 ± 8
Globules	7 ± 1	46 ± 7	47 ± 7	4 ± 1	48 ± 7	48 ± 7	3 ± 1	49 ± 7	49 ± 7

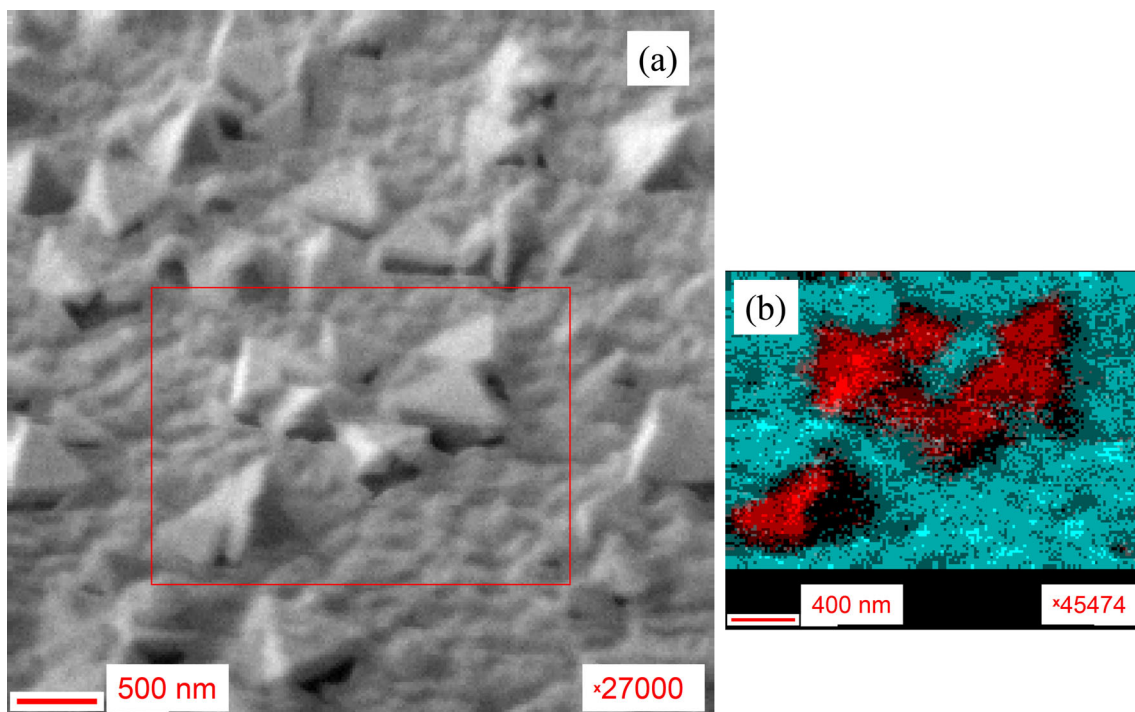


Fig. 7 SEM image (a) with a highlighted mapping area and AES map (b) of the distribution of cadmium (blue) and lead (red) atoms for the two-phase composition $\text{Cd}_{0.071}\text{Pb}_{0.929}\text{S}/\text{Cd}_{1-\delta}\text{S}$ (Color figure online)

when we go from using $\text{Cd}(\text{CH}_3\text{COO})_2$ to $\text{Cd}(\text{NO}_3)_2$ and then to CdSO_4 .

The predominant content of lead in the crystallites and cadmium in the sublayer is confirmed by the AES-map of the distribution of the ions shown in Fig. 7, where lead atoms are shown by red color and cadmium atoms are shown by blue one. From comparison with the SEM image of the same part of the film it is seen that the light large crystallites consist of lead sulfide mainly and the place between them mainly contains cadmium sulfide. One can notice that the concentration of the cadmium in the films determined by the Auger spectroscopy is close to that estimated by EDX within error of the both methods.

3.4 Raman spectroscopy

The Raman spectra of the binary PbS and CdS films and, as an example, the two-phase $\text{Cd}_x\text{Pb}_{1-x}\text{S}/\text{Cd}_{1-\delta}\text{S}$ composition deposited from the reaction bath with cadmium acetate are shown in Fig. 8. As it is known, the position and shape of the lines in the Raman spectra depend on the molecular structure of the compound. Generally, the spectrum of a crystalline material shows sharp and intense Raman

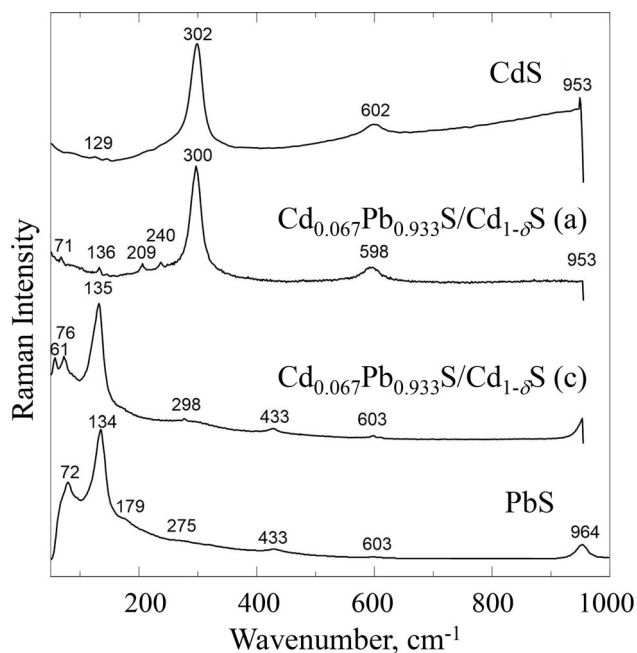


Fig. 8 Raman spectra of PbS, CdS films, and two-phase composition $\text{Cd}_{0.067}\text{Pb}_{0.933}\text{S}/\text{Cd}_{1-\delta}\text{S}$ of the amorphous layer (a) and crystallite (c)

peaks while an amorphous or polycrystalline sample presents broad and less intense Raman peaks [44].

The spectrum of the PbS film indicates the presence of seven vibrational active Raman modes with centers at about 72, 134, 179, 275, 433, 603, and 964 cm^{-1} [45–47]. For the high-symmetric cubic $B1$ structure ($Fm\bar{3}m$ space group) of the PbS film, the spectrum contains an intense peak at 133 or 134 cm^{-1} , which is responsible for the combination of the longitudinal and transverse acoustic modes (LA+TA), as it was shown in [48–53]. The low-frequency mode at 72 cm^{-1} can be attributed to the transverse optical (TO) mode [51]. A close value of the phonon frequency (73 cm^{-1}) in the Raman spectrum was reported in [52], and the peak at about 78 cm^{-1} , attributed to the A_{1g} mode in PbS film, was observed in [46]. The weak Raman scattering line at a frequency of 179 cm^{-1} in the spectrum of the PbS film belongs to the longitudinal optical (LO) mode, while the lines near 430 and 600 cm^{-1} originate from the first and second overtones of the main LO phonon modes of PbS, respectively [50]. The weak peak at about 275 cm^{-1} is attributed to two-phonon processes ($2 \times 134 = 268 \text{ cm}^{-1}$) in PbS and in our case is slightly shifted to the high-frequency region [52, 54].

For the CdS film, the most intensive mode is observed at a frequency of 302 cm^{-1} and is associated with the LO phonons [54–56]. In addition to this peak, a line of overtones of the LO phonon with a reduced intensity appears at the doubled frequency 2LO (at $\sim 602 \text{ cm}^{-1}$), which is in agreement with the literature data [57, 58].

An analysis of the Raman spectra of the two-phase composition synthesized with adding $\text{Cd}(\text{CH}_3\text{COO})_2$ shows a change in the relative intensity, broadening of the emission peaks and their shift as a result of the formation of both a solid solution (line *c* in Fig. 8) and an amorphous phase (line *a*) located in the sublayer. It is known [59] that a change in the unit cell parameter upon substitution of one ion for another (a change in the average radius of the cation sublattice) results in a shift of the frequency of the optical phonon confirming formation the solid solution. The difference in ionic radii ($\sim 24\%$) and atomic masses ($\sim 84\%$) for Pb^{2+} and Cd^{2+} pair, as well as the microstrains caused by the difference in the values of the crystal lattice constants of the PbS film (0.59348(1) nm) and CdS film (0.546 nm) influences the position of the lines in the Raman spectra. In the Raman spectrum corresponding to the crystallites (line *c* in Fig. 8), there are intensive peaks at 76 and 135 cm^{-1} ,

which are in fact the vibrational modes (72, 134 cm^{-1}) typical for lead sulfide but shifted towards the high-frequency region. In the spectrum obtained for the amorphous sublayer (line *a* in Fig. 8), the dominant band has the frequency corresponding to CdS (300 cm^{-1}) [60]. Besides this a weak Raman line is found at 598 cm^{-1} , which is near the doubled frequency 2LO (at $\sim 602 \text{ cm}^{-1}$) in the CdS structure, and very weak peaks at frequencies of 71 and 136 cm^{-1} , which are characteristic of microcrystalline PbS. The peaks at 209 and 240 cm^{-1} with the pronounced dispersions are the characteristic longitudinal modes of the optical phonons of the first and second orders, which are identified in Ref. [61] as surface phonon modes appeared upon excitation by a laser with a wavelength of 514.5 nm. Therefore, the Raman spectra convincingly confirm the presence in the two-phase composition of a substitutional solid solution, as well as an individual phase of cadmium sulfide.

3.5 Diffuse reflectance spectroscopy

As is known, an important characteristic for semiconductor compounds is the band gap; therefore, one of the aims of the present work was to estimate it for the films under study. The diffuse reflection spectra $R(\lambda)$ of the semiconductor two-phase $\text{Cd}_x\text{Pb}_{1-x}\text{S}/\text{Cd}_{1-\delta}\text{S}$ compositions are shown in Fig. 9a. Note that the optical characteristics of the films are close. The maximum value of the diffuse reflection ($R = 62\text{--}67\%$) is recorded in the low-energy spectral range at wavelengths $\lambda \sim 1935 \text{ nm}$. As the energy increases, a stepwise decrease in R occurs. The most pronounced drop in the diffuse reflectance is observed in two spectral ranges: 455–580 nm (2.14–2.73 eV) and 1520–1800 nm (0.69–0.82 eV), which is associated with the inhomogeneity of the chemical composition of the films. These energy ranges were further studied in detail in order to determine the band gap of the two-phase $\text{Cd}_x\text{Pb}_{1-x}\text{S}/\text{Cd}_{1-\delta}\text{S}$ compositions. In the region of 200–450 nm for all two-phase films under study significant absorption of incident radiation occurs and the value of R becomes close to zero.

The Kubelka–Munk function (2) was calculated from the diffuse reflectance data and the dependences $[F(R_\infty)/hv]^2 = f(hv)$ are plotted in Fig. 9b and c. In the case of the direct allowed transitions, the extrapolation of the linear sections of the curves to

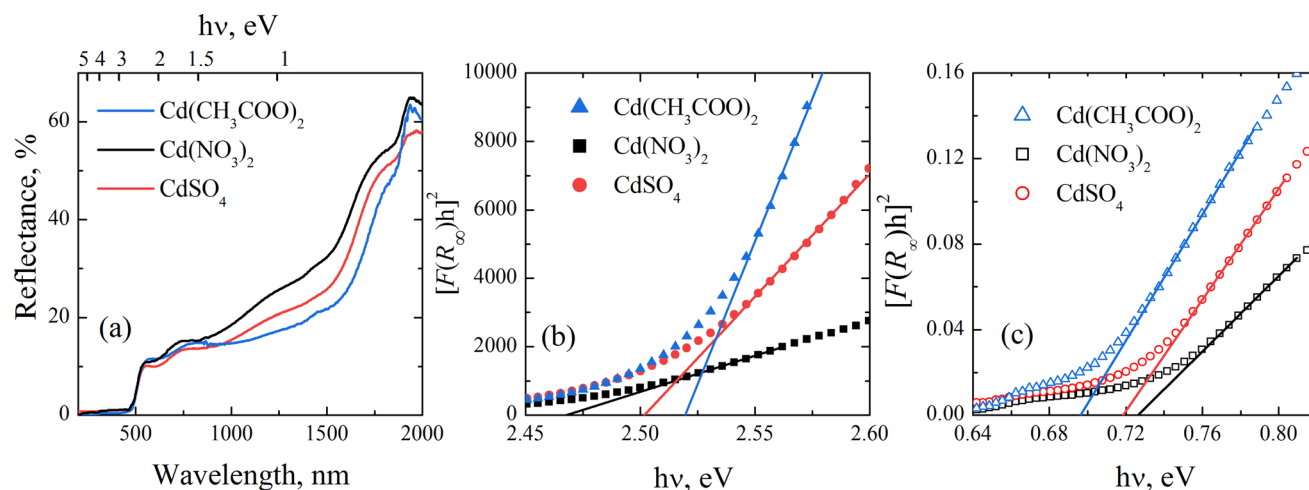


Fig. 9 Diffuse reflectance spectra (a) and results of graphical determination of the band gap (b, c) of two-phase $\text{Cd}_x\text{Pb}_{1-x}\text{S}/\text{Cd}_{1-\delta}\text{S}$ compositions deposited from the bath containing $\text{Cd}(\text{NO}_3)_2$, CdSO_4 , $\text{Cd}(\text{CH}_3\text{COO})_2$

the abscissa axis made it possible to determine the value of the band gap E_g . It is seen, that for all the films deposited in the presence of the cadmium salt it is possible to find two values of E_g , which vary in the ranges of 2.47–2.52 eV and 0.69–0.73 eV indicating the two-phase composition of the films. It is known from the literature that the band gap for a single crystal and thin-film of CdS is 2.42 eV [3, 62, 63], while for lead sulfide E_g is 0.41 eV [1, 2]. It was found in a number of works that, in the case of nanostructured CdS films, a significant increase in the band gap can be observed up to 2.57 eV due to the quantum size effect [64, 65]. Comparison of our results with the literature data allows us to state that in the two-phase compositions one of the phases is close to CdS.

The band gap interval of 0.69–0.73 eV corresponds to the band gap of $\text{Cd}_x\text{Pb}_{1-x}\text{S}$ solid solutions located on the amorphous phase of cadmium sulfide. Using the linear dependence of the band gap on the cadmium content in the synthesized $\text{Cd}_x\text{Pb}_{1-x}\text{S}$ solid solutions, the compositions of the deposited solid solutions can be estimated. The determined content of cadmium in $\text{Cd}_x\text{Pb}_{1-x}\text{S}$ is about $x = 0.14$ for the film deposited with adding $\text{Cd}(\text{CH}_3\text{COO})_2$, $x = 0.15$ for film deposited with $\text{Cd}(\text{NO}_3)_2$, and $x = 0.16$ for CdSO_4 . The estimated concentrations of cadmium in the solid solutions are close to the results obtained by the EDX analysis.

Thus, the complex studies carried out using the X-ray diffraction, EDX analysis, Auger, Raman, and diffuse reflectance spectroscopies confirm that our fabrication protocol yields two-phase compositions

consisting of the substitutional solid solutions ($\text{Cd}_{0.067}\text{Pb}_{0.933}\text{S}$, $\text{Cd}_{0.071}\text{Pb}_{0.929}\text{S}$, or $\text{Cd}_{0.076}\text{Pb}_{0.924}\text{S}$) and the individual $\text{Cd}_{1-\delta}\text{S}$ phase, which differ in their semiconducting and photoelectric properties [66, 67]. As noted in [66], the photodetectors based on p -type $\text{Cd}_x\text{Pb}_{1-x}\text{S}$ solid solutions are characterized by a high photoresponse in the visible and near-infrared ranges and high stability of the photoelectric characteristics. Note also that in contrast to the studied substitutional solid solutions, cadmium sulfide is characterized by a pronounced n -type of conductivity. In the future, this makes it possible in one technological stage to form two-phase compositions and heterostructures that can be used in the creation of the solar radiation converters.

4 Conclusions

As a result of complex comparative studies using the methods of X-ray diffraction, EDX analysis, Auger, Raman, and diffuse reflectance spectroscopies, the thin-film two-phase $\text{Cd}_x\text{Pb}_{1-x}\text{S}/\text{Cd}_{1-\delta}\text{S}$ compositions chemically deposited using cadmium acetate, nitrate and sulfate were studied. According to the change in the lattice period determined from minimizing the XRD patterns, the following estimates of the compositions of the synthesized solid solutions were made: $\text{Cd}_{0.067}\text{Pb}_{0.933}\text{S}$ ($\text{Cd}(\text{CH}_3\text{COO})_2$), $\text{Cd}_{0.071}\text{Pb}_{0.929}\text{S}$ ($\text{Cd}(\text{NO}_3)_2$), $\text{Cd}_{0.076}\text{Pb}_{0.924}\text{S}$ (CdSO_4). In the series from cadmium acetate to cadmium sulfate, a decrease in the size of the coherent scattering regions of the

$\text{Cd}_x\text{Pb}_{1-x}\text{S}$ solid solution from ~ 1000 nm to 312 nm was found, and in the $(\text{Cd}_{1-\delta}\text{S})$ phase from 33.0 to 7.5 nm. The calculated value of microstrains $\Delta d/d$ in the mentioned sequence of films increases from 16.1×10^{-4} to 28.5×10^{-4} and 27.8×10^{-4} , respectively. The revealed differences are the result of the influence of the nucleophilicity of the anionic component of cadmium salts on the kinetics of thiourea decomposition. The data of elemental EDX analysis and Auger spectroscopy of the films synthesized with adding cadmium salt confirm the nonstoichiometric character of the local distribution of the main elements (Pb, Cd, S) between the crystallites, globular formations, and intercrystalline space. In this case, well-faceted crystallites in their composition are the substitutional solid solutions, formation of which is confirmed also by the shift of the Raman lines. The total cadmium content in the films, established by both Auger spectroscopy and EDX analysis, turned out to be higher than in the composition of solid solutions estimated from the change in the lattice period, which indicates possible interstitial position of the part of cadmium ions. The presence of the amorphous cadmium sulfide phase being a sublayer in the films is determined from the comparison of the SEM images and Auger data. The E_g values determined from the optical data of the films vary in the ranges 2.47–2.52 eV and 0.69–0.73 eV, which indicates the two-phase composition of the synthesized films. In this case, the higher E_g values belong to cadmium sulfide, and the lower ones correspond to the band gap of the $\text{Cd}_x\text{Pb}_{1-x}\text{S}$ solid solutions located on the sublayer of the amorphous phase of cadmium sulfide. Thus, the complex studies carried out have confirmed the chemical synthesis of the two-phase $\text{Cd}_x\text{Pb}_{1-x}\text{S}/\text{Cd}_{1-\delta}\text{S}$ films, which differ in their composition depending on the cadmium salts used, as well as in their semiconducting properties. In the future, this gives an opportunity in one technological stage to form the compositions and heterostructures that can be used in the creation of the solar radiation converters.

Acknowledgements

The research was financially supported in part by 211 Program of the Government of the Russian Federation (No. 02.A03.21.0006), was carried out within the state assignment of Ministry of Science and Higher

Education of the Russian Federation (Themes No. AAAA-A18-118020190112-8 (“Flux”), No. AAAA-A18-118020290104-2 (“Spin”), and No. AAAA-A19-119031890025-9) and in part supported by RFBR (projects No. 18-29-11051-mk, 20-48-660041-r-a).

Author contributions

Conceptualization: LNM, VFM; methodology: LNM, VFM; formal analysis and investigation: IVV, VIV, OAL, EVM, VSB, INM; writing—original draft preparation: LNM, VIV, EVM; writing—review and editing: LNM, VFM, VIV, EVM.

Funding

The research was financially supported in part by 211 Program of the Government of the Russian Federation (No. 02.A03.21.0006), was carried out within the state assignment of Ministry of Science and Higher Education of the Russian Federation (Themes No. AAAA-A18-118020190112-8 (“Flux”), No. AAAA-A18-118020290104-2 (“Spin”), and No. AAAA-A19-119031890025-9) and in part supported by Russian Foundation for Basic Research (projects No. 18-29-11051-mk, 20-48-660041-r-a).

Data availability

The authors declare that the data supporting the findings of this study are available within the article.

Declarations

Conflict of interest The authors declared that they have no conflict of interest.

References

1. N.K. Abrikosov, L.E. Shelimova, *Semiconductor Materials Based on IV–VI Compounds* (Nauka, Moscow, 1975). (in Russian)
2. V.I. Kaidanov, Y.I. Ravich, *Sov. Phys. Usp.* **28**, 31 (1985). <https://doi.org/10.1070/PU1985v028n01ABEH003632>
3. S. Kumar, B. Bhattacharya, *Ind. J. Pure Appl. Phys.* **43**, 609 (2005)
4. D.A. Caselli, C.Z. Ning, *Opt. Express.* **19**, A686 (2011). <https://doi.org/10.1364/OE.19.00A686>

5. Y.B. Castillo-Sanchez, L.A. Gonzalez, *Mater. Sci. Semicond. Process.* **121**, 105405 (2021). <https://doi.org/10.1016/j.mssp.2020.105405>
6. T.O. Boykin II., N. Dhakal, J. Boroumand, F. Javier Gonzalez, I.O. Oladeji, P. Figueiredo, S. Neushul, R.E. Peale, *MRS Adv.* **2**, 2013 (2020). <https://doi.org/10.1557/adv.2020.324>
7. M.K.A. Mohammed, *Plasmonics* **15**, 1989 (2020). <https://doi.org/10.1007/s11468-020-01224-5>
8. E.M. Nasir, I.S. Naji, *Aust. J. Basic Appl. Sci.* **9**, 364 (2015)
9. M. Kamruzzaman, R. Dutta, J. Podder, *Semiconductors* **46**, 957 (2012). <https://doi.org/10.1134/S1063782612070111>
10. L.N. Maskaeva, N.A. Forostyanaya, V.F. Markov, V.I. Voronin, *Russ. J. Inorg. Chem.* **60**, 552 (2015). <https://doi.org/10.1134/S0036023615050150>
11. M. Gugliemi, A. Martucci, J. Fick, G. Vitrant, *J. Sol-Gel Sci. Technol.* **11**, 229 (1997). <https://doi.org/10.1023/A:1008650027769>
12. R.D. Muhamediarov, G.A. Kitaev, V.M. Markova, V.I. Stuk, *Inorg. Mater.* **17**, 1739 (1981). (**in Russian**)
13. G.A. Kitaev, V.F. Markov, L.N. Maskaeva, L.E. Vasyunina, I.V. Shilova, *Inorg. Mater.* **26**, 202 (1990)
14. L.N. Maskaeva, V.F. Markov, A.I. Gusev, *Russ. J. Inorg. Chem.* **49**, 1065 (2004)
15. I.V. Vaganova, L.N. Maskaeva, V.F. Markov, V.I. Voronin, V.G. Bamburov, *Nanosystems* **9**, 811 (2018). <https://doi.org/10.17586/2220-8054-2018-9-6-811-822>
16. E. Pentia, V. Draghici, G. Sarau, B. Mereu, L. Pintilie, F. Sava, M. Popescu, *J. Electrochem. Soc.* **151**, G729 (2004). <https://doi.org/10.1149/1.1800673>
17. E. Rabinovich, E. Wachtel, G. Hodes, *Thin Solid Films* **517**, 737 (2008). <https://doi.org/10.1016/j.tsf.2008.08.162>
18. L.N. Maskaeva, A.V. Pozdin, V.F. Markov, V.I. Voronin, *Semiconductors* **54**, 1567 (2020). <https://doi.org/10.1134/S1063782620120209>
19. A.K.E. Suryavanshi, R.B. Dhake, A.M. Patil, M.R. Sonawane, *Optik* **218**, 165008 (2020). <https://doi.org/10.1016/j.ijleo.2020.165008>
20. G.B. Reddy, D.K. Pandya, K.L. Chopra, *Sol. Energy Mater.* **15**, 383 (1987). [https://doi.org/10.1016/0165-1633\(87\)90058-X](https://doi.org/10.1016/0165-1633(87)90058-X)
21. S.R. Deo, A.K. Singh, L. Deshmukh, L.J. Paliwal, R.S. Singh, *Optik* **126**, 2311 (2015). <https://doi.org/10.1016/j.ijleo.2015.05.130>
22. M.A. Barote, S.S. Kamble, A.A. Yadav, R.V. Suryavnsi, L.P. Deshmukh, E.U. Masumdar, *Mater. Lett.* **78**, 113 (2012). <https://doi.org/10.1016/j.matlet.2012.03.018>
23. L.N. Maskaeva, V.F. Markov, A.I. Gusev, *Dokl. Phys. Chem.* **390**, 147 (2003). <https://doi.org/10.1023/A:1024446709437>
24. H.M. Rietveld, *J. Appl. Crystallogr.* **2**, 65 (1969). <https://doi.org/10.1107/S0021889869006558>
25. D.L. Bush, J.E. Post, *Rev. Mineral.* **20**, 369 (1990). <https://doi.org/10.1180/claymin.1990.025.4.12>
26. J. Rodrigues-Carvajal, *Phys. B* **192**, 55 (1993). [https://doi.org/10.1016/0921-4526\(93\)90108-1](https://doi.org/10.1016/0921-4526(93)90108-1)
27. G.K. Williamson, W.H. Hall, *Acta. Metall.* **1**, 22 (1953). [https://doi.org/10.1016/0001-6160\(53\)90006-6](https://doi.org/10.1016/0001-6160(53)90006-6)
28. P. Kubelka, F. Munk, *Techn. Physik.* **12**, 593 (1931) [in German]. See also English translation by S. Westin (An article on optics of paint layers, <http://www.graphics.cornell.edu/~westin/pubs/kubelka.pdf>)
29. E. Cruceanu, D. Niculescu, *Comptes Rendus Hebdomadaires des Seances de l'Academie des Sciences* **261**, 935 (1965)
30. H. Sowa, *Solid State Sci.* **7**, 73 (2005). <https://doi.org/10.1016/j.solidstatesciences.2004.10.011>
31. S. Ruben, *Handbook of Elements* (Open Court Publishing, La Salle, 1985)
32. L. Vegard, *Z. Phys.* **5**, 17 (1921). <https://doi.org/10.1007/BF01349680>
33. T. Kobayashi, K. Susa, S. Taniguchi, *J. Phys. Chem. Solids* **40**, 781 (1979). [https://doi.org/10.1016/0022-3697\(79\)90160-4](https://doi.org/10.1016/0022-3697(79)90160-4)
34. J.A. Corll, *J. Appl. Phys.* **35**, 3032 (1964). <https://doi.org/10.1063/1.1713151>
35. C.J.M. Rooymans, *Phys. Lett.* **4**, 186 (1963). [https://doi.org/10.1016/0031-9163\(63\)90356-1](https://doi.org/10.1016/0031-9163(63)90356-1)
36. K. Susa, T. Kobayashi, S. Taniguchi, *J. Solid State Chem.* **33**, 197 (1980). [https://doi.org/10.1016/0022-4596\(80\)90120-6](https://doi.org/10.1016/0022-4596(80)90120-6)
37. V.F. Markov, L.N. Maskaeva, *Russ. Chem. Bull.* **63**, 1523 (2014). <https://doi.org/10.1007/s11172-014-0630-7>
38. T. Ungar, I. Dragomir, A. Revesz, A. Borbely, *J. Appl. Crystallogr.* **32**, 992 (1999). <https://doi.org/10.1107/S0021889899009334>
39. T. Ungar, A. Borbely, *Appl. Phys. Lett.* **69**, 3173 (1996). <https://doi.org/10.1063/1.117951>
40. A.V. Volkov, V.N. Vigdorovich, D.P. Kolesnikov, *Phys. Technol. Semicond.* **21**, 90 (1987). (**in Russian**)
41. N.C. Sharma, D.K. Pandya, H.K. Sehgal, K.L. Chopra, *Thin Solid Films* **42**, 383 (1977). [https://doi.org/10.1016/0040-6090\(77\)90373-X](https://doi.org/10.1016/0040-6090(77)90373-X)
42. L.E. Davis, N.C. MacDonald, P.W. Palmberg, G.E. Riach, R.E. Weber, *Handbook of Auger Electron Spectroscopy* (Physical Electronics Division PerkinElmer Corporation, Eden Prairie, 1976)
43. J. Morimoto, *Jpn. J. Appl. Phys.* **19**, L296 (1980). <https://doi.org/10.1143/JJAP.19.L296>
44. J.-H. Chen, C.-G. Chao, J.-C. Ou, T.-F. Liu, *Surf. Sci.* **601**, 5142 (2007). <https://doi.org/10.1016/j.susc.2007.04.228>
45. M. Hangyo, S. Nakashima, Y. Hamada, T. Nishio, Y. Ohno, *Phys. Rev. B* **48**, 11291 (1993). <https://doi.org/10.1103/PhysRevB.48.11291>

46. M. Kul, Anadolu Univ. J. Sci. Technol. B 7, 46–58 (2019). <https://doi.org/10.20290/aubtdb.465445>
47. S.V. Ovsyannikov, V.V. Shchennikov, A. Cantarero, A. Cros, A.N. Titov, J. Mater. Sci. Eng. 462, 422 (2007). <https://doi.org/10.1016/j.msea.2006.05.175>
48. H. Cao, G. Wang, S. Zhang, X. Zhang, Nanotechnology 17, 3280 (2006). <https://doi.org/10.1088/0957-4484/17/13/034>
49. R. Sherwin, R.J.H. Clark, R. Lauck, M. Cardona, Solid State Commun. 134, 565 (2005). <https://doi.org/10.1016/j.ssc.2005.02.026>
50. G.D. Smith, S. Firth, R.J.H. Clark, M. Cardona, J. Appl. Phys. 92, 4375 (2002). <https://doi.org/10.1063/1.1505670>
51. T. Tohidi, K. Jamshidi-Ghaleh, A. Namdar, R. Abdi-Ghaleh, Mater. Sci. Semicond. Process. 25, 197 (2014). <https://doi.org/10.1016/j.mssp.2013.11.028>
52. T.D. Krauss, F.W. Wise, D.B. Tanner, Phys. Rev. Lett. 76, 1376 (1996). <https://doi.org/10.1103/PhysRevLett.76.1376>
53. L.N. Maskaeva, V.F. Markov, V.I. Voronin, A.I. Gusev, Thin Solid Films 461, 325 (2003). <https://doi.org/10.1016/j.tsf.2004.02.035>
54. A.A. Milekhin, L. Sveshnikova, T. Duda, N. Surovtsev, S. Adichtchev, D.R.T. Zahn, Chin. J. Phys. 49, 63–70 (2011)
55. A.I. Belogorokhov, I.A. Belogorokhov, R.P. Miranda, M.I. Vasilevskii, S.A. Gavrilov, JETP 104, 111 (2007). <https://doi.org/10.1134/S1063776107010128>
56. A.G. Rolo, M.I. Vasilevskiy, J. Raman Spectrosc. 38, 618 (2007). <https://doi.org/10.1002/jrs.1746>
57. M.I. Vasilevskiy, Phys. Rev. B. 66, 195326 (2002). <https://doi.org/10.1103/PhysRevB.66.195326>
58. J.O. Oladeji, L. Chow, J.R. Liu, W.K. Chu, A.N.P. Bustamante, C. Fredricksen, A.F. Schulte, Thin Solid Films 359, 154 (2000). [https://doi.org/10.1016/S0040-6090\(99\)00747-6](https://doi.org/10.1016/S0040-6090(99)00747-6)
59. V.S. Kurnosov, V.V. Pishko, V.V. Tsapenko, Low Temp. Phys. 33, 872 (2007). <https://doi.org/10.1063/1.2796155>
60. J. Trajic, M. Gilic, N. Romcevic, M. Romcevic, Sci. Sinter. 47, 145 (2015). <https://doi.org/10.2298/SOS1502145T>
61. K.K. Nanda, S.N. Sahu, R.K. Soni, S. Tripathy, Phys. Rev. B 58, 15405 (1998). <https://doi.org/10.1103/PhysRevB.58.15405>
62. A. Mukherjee, M.R. Das, A. Banerjee, P. Mitra, Thin Solid Films 704, 138005 (2020). <https://doi.org/10.1016/j.tsf.2020.138005>
63. N.A. Forostyanaya, L.N. Maskaeva, Z.I. Smirnova, S. Santra, G.V. Zyryanov, V.F. Markov, M.V. Kuznetsov, Thin Solid Films 657, 101 (2018). <https://doi.org/10.1016/j.tsf.2018.04.031>
64. D. Kaushik, R.R. Singh, M. Sharma, D.K. Gupta, N.P. Lalla, R.K. Pandey, Thin Solid Films 515, 7070 (2007). <https://doi.org/10.1016/j.tsf.2007.02.093>
65. S. Chander, M.S. Dhaka, Thin Solid Films 638, 179 (2017). <https://doi.org/10.1016/j.tsf.2017.07.048>
66. L.N. Maskaeva, V.F. Markov, M.Y. Porkhachev, O.A. Mokrousova, Fire Explos. 24, 67–73 (2015). <https://doi.org/10.18322/PVB.2015.24.09.67-73>
67. A.E. Bezdetnova, V.F. Markov, L.N. Maskaeva, Yu.G. Shashmurin, A.S. Frants, T.V. Vinogradova, J. Anal. Chem. 74, 1256 (2019). <https://doi.org/10.1134/S1061934819120025>

Publisher's Note Springer Nature remains neutral with regard to jurisdictional claims in published maps and institutional affiliations.